Motion analysis within non-rigid body objects in satellite images using least squares matching

M. Hasanlou and M.R. Saradjian

Remote Sensing Division, Surveying and Geomatics Engineering Dept.,
Faculty of Engineering, University of Tehran, Tehran, Iran
mhasanlou@geomatics.ut.ac.ir and sarajian@ut.ac.ir

ABSTRACT:

Using satellite images, an optimal solution to water motion has been presented in this study. Since temperature patterns are suitable tracers in water motion, Sea Surface Temperature (SST) images of Caspian Sea taken by MODIS sensor on board Terra satellite have been used in this study. Two daily SST images with 24 hours time interval are used as input data.

Computation of templates correspondence between pairs of images is crucial within motion algorithms using non-rigid body objects. Image matching methods have been applied to estimate water body motion within the two SST images. The least squares matching technique, as a flexible technique for most data matching problems, offers an optimal spatial solution for the motion estimation. The algorithm allows for simultaneous local radiometric correction and local geometrical image orientation estimation. Actually, the correspondence between the two image templates is modeled both geometrically and radiometrically. Geometric component of the model includes six geometric transformation parameters and radiometric component of the model includes two radiometric transformation parameters. Using the algorithm, the parameters are automatically corrected, optimized and assessed iteratively by the least squares algorithm. The method used in this study, has presented more efficient and robust solution compared to the traditional motion estimation schemes.

KEY WORDS: Least squares image matching, Non-rigid body motion, Satellite Sea Surface Temperature images, MODIS data

1. INTRODUCTION

Oceanographic and atmospheric images obtained from environmental satellites present a new challenge for geosciences. The wide ranges of remote sensors allow characterizing natural phenomena through different physical measurements. For instance Sea Surface Temperature (SST) images, altimetry data and ocean color data can be used simultaneously for characterizing currents and vortex structures in the ocean.

A major advantage of environmental remote sensing is the regular sampling of the measurements and their availability. These regular temporal and spatial data samplings allow characterizing the short range evolution of atmospheric and oceanographic processes with image sequence processing.

The purpose of this paper is to derive a relatively complete framework for processing large dynamic oceanographic and atmospheric image sequences in order to detect global displacements such as oceanographic streams, cloud motion, or to localize particular structures like motion current and vortices and fronts. These characterizations will help in initializing particular processes in a global monitoring system.

Processing such image sequences raise some specific problems. Indeed, computing an apparent motion field to characterize short range evolution must take into account discontinuities of the motion field that occur near SST temperature fronts. For this purpose, least squares image matching method has been used to solve the apparent motion which involves radiometric corrections and local geometrical image shaping allowing flow discontinuities.

The outline of the rest of this paper is as follows. In section 2 a brief introduction to least squares matching is presented. Section 3 describes modifications of the method concerned with variations in the number of parameters used. This aims to improve the result of optical flow calculation. Section 4 presents results of experiments that verify the effectiveness of our proposed approach. The conclusion is given in section 5.

2. LEAST SQUARES MATCHING

Image matching is a key component in almost all image analysis processes regarding a wide range of applications such as motion analysis, computer vision, robotics, navigation, automatic surveillance and etc. [Gruen,1985]Cross-correlation and related techniques have dominated the field since the early fifties. The shortcomings of this class of image matching methods have caused a slow-down in the development of operational automated correlation systems. Illumination and reflectance conditions might distort the images radiometrically. Under certain conditions this could even cause a geometrical displacement. Noise from the electrical components and the sampling rate (pixel size) could also influence both the geometrical and the radiometric correspondence of the images. Cross-correlation works fast and well if the patches to be matched contain enough signal without too much high frequency content and under assumption that geometrical and radiometric distortions are minimum. The latter two conditions are rarely met in remotely sensed images.

In the conventional approach [Ackermann, 1988] to least squares matching (LSM), the correspondence between two image fragments is modeled by a geometric model (six parameters transformation) and a radiometric model (two parameters transformation). Pixel gray values in one image (called left image in this paper) are arbitrarily chosen to be the observables, while pixel gray

values in the other image (right image) are chosen to be constants. Experience has shown that the alignment/ correspondence between two images to be matched generally have to be within a few pixels otherwise the process will not converge. This is more restrictive than other matching methods, and therefore requires good approximation of matching window when using least squares methods.

2.1 Formulation

A simplified condition equation, considering only the geometric parameters would be,

$$g(x,y) = h(x',y') \tag{1}$$

In which the two coordinate systems are related by six parameters transformation,

$$\begin{aligned} x' &= a_1 x + a_2 y + a_3 \\ y' &= b_1 x + b_2 y + b_3 \end{aligned} \tag{2}$$

An extended model including two radiometric parameters for contrast and brightness (or equivalently gain and offset) would be,

$$g(x,y) = k_1 h(x',y') + k_2 \tag{3}$$

Written in the form of a condition equation it becomes,

$$F = g(x,y) - k_1 h(x',y') - k_2 = 0 \tag{4}$$

Where $a_1, a_2, a_3, b_1, b_2, b_3, k_1, k_2$ are the parameters, g represents the observation, x, y are constant values, and h is a constant. This equation can be linearized into the form:

$$V + B\Delta = f \tag{5}$$

Since it is assumed that the images are nearly aligned and are radiometrically similar, one can take the initial approximation parameter vector to be,

$$\begin{aligned} &[a_1^o \quad a_2^o \quad a_3^o \quad b_1^o \quad b_2^o \quad b_3^o \quad k_1^o \quad k_2^o]^T \\ &= [1 \quad 0 \quad 0 \quad 0 \quad 1 \quad 0 \quad 1 \quad 0]^T \end{aligned} \tag{6}$$

The coefficients of the matrix B will consist of partial derivatives of equation (4).

$$B = [\frac{\partial F}{\partial a_1} \quad \frac{\partial F}{\partial a_2} \quad \frac{\partial F}{\partial a_3} \quad \frac{\partial F}{\partial b_1} \quad \frac{\partial F}{\partial b_2} \quad \frac{\partial F}{\partial b_3} \quad \frac{\partial F}{\partial k_1} \quad \frac{\partial F}{\partial k_2}] \tag{7}$$

These can be developed as follows,

$$\frac{\partial F}{\partial a_1} = -k_1 \frac{\partial h}{\partial a_1} = -k_1 \frac{\partial h}{\partial x'} \frac{\partial x'}{\partial a_1} = -h_x x \tag{8}$$

Where we evaluated the expression at the initial approximations, and for notational compactness we adopt,

$$h_x = \frac{\Delta h}{\Delta x} \approx \frac{\partial h}{\partial x} \quad h_y = \frac{\Delta h}{\Delta y} \approx \frac{\partial h}{\partial y} \tag{9}$$

In practice, these are computed using gray values from the right image as follows,

$$\begin{aligned} h_x &= \frac{h(x'+1,y') - h(x'-1,y')}{2} \\ h_y &= \frac{h(x',y'+1) - h(x',y'-1)}{2} \end{aligned} \tag{10}$$

It should be noted that h_x represents a derivative, whereas $h(x',y')$ represents a gray value in the right image.

$$\frac{\partial F}{\partial a_2} = -k_1 \frac{\partial h}{\partial a_2} = -k_1 \frac{\partial h}{\partial x'} \frac{\partial x'}{\partial a_2} = -h_x y \tag{11}$$

$$\frac{\partial F}{\partial a_3} = -k_1 \frac{\partial h}{\partial a_3} = -k_1 \frac{\partial h}{\partial x'} \frac{\partial x'}{\partial a_3} = -h_x \tag{12}$$

By similar analysis,

$$\begin{aligned} &\frac{\partial F}{\partial b_1} = -h_y x \quad \frac{\partial F}{\partial b_2} = -h_y y \quad \frac{\partial F}{\partial b_3} = -h_y \\ &\frac{\partial F}{\partial k_1} = -h(x',y') \quad \frac{\partial F}{\partial k_2} = -1 \end{aligned} \tag{13}$$

The term f, the right hand side term in Eq. (5) is,

$$f = -F = -(g(x,y) - k_1 h(x',y') - k_2) \tag{14}$$

Which when evaluated at the approximations (the identity transformation), it becomes:

$$f = h(x,y) - g(x,y) \tag{15}$$

2.2 LSM Procedure

The resulting normal equations may be formed sequentially, avoiding the actual formation of the full condition equations. They are then solved for the parameter corrections. For the second and subsequent iterations, we resample the right image, $h(x',y')$ using the inverse transformation defined by the updated six parameters. After several iterations and resampling, the two images should appear to be aligned and registered. Following are a few practical hints:

- Update parameters just like nonlinear least squares, *i.e.* $a^1 = a^0 + \delta a$.
- Convergence occurs when $\Delta \to 0$.
- The matrix B and vector f are computed from the resampled right image.
- The right image is resampled in every iteration, following the first, usually by bilinear interpolation.

3. IMPLEMENTATION

In principle, temperature patterns are suitable tracers for water motion analysis. Therefore, water motion in satellite images has been depicted using SST images as input data which are two daily SST images with 24 hours time interval of Caspian Sea taken by MODIS sensor on board Terra satellite. The process begins with registration of the two images. Registration is important

step to extract optical flow using least squares matching, because quality of approximation of initial value of matching window location in right image effects the convergence or divergence of the algorithm. The second step is to mask out coastal area due to their pixel values' negative impact on the convergence of the least squares matching algorithm. In the next step, initial values for geometric and radiometric parameters being used are set. In this step, the number of iterations is also specified. Then a threshold value is set to check all iterations when LSM reaches to a proper solution. In this study, 30 iterations have been used mostly in all computations and threshold value is $\Delta = 0.001$. When either of these criteria is met, computation stops and algorithm saves the optical flow results. Template size used is 31×31 for both template and matching window in the search area.

4. EXPERIMENTAL RESULT

First, the performance of the algorithm has been examined on simulated water motion in sequences of SST images for which 2D motion fields are known. Then, the performance has been examined on real water motion in the image sequences. In the next section, the image sequence used and angular measures of error are described.

4.1 Water motion simulation in SST sequences

The advantages of using simulation data are their known 2D motion fields and that the scene properties can be controlled and tested when varying the parameters. In addition, the signal content of image is real signal that is taken by MODIS sensor in thermal bands. The water motion simulation in image sequences is made by sinusoidal transformation that consist of two sinusoidal in x and y directions shown in Eq. (16).

$$X = x_i + 5\sin(2\pi x_i / imagewidth)$$
$$Y = y_i - 3\sin(2\pi y_i / imagewidth) \quad (16)$$

By applying the transformation to an image and resampling it by bilinear resampling method, another image with known displacements in all pixels relevant to the first one is generated. Figure 1 illustrates result of optical flow in dataset on the first and synthetically transformed images.

4.2 Real water motion in SST sequences

A sequence of two real SST images of Caspian Sea taken by MODIS sensor is used. The images have been registered first and then the coastal area and cloud pixels have been removed. Figure 2 shows the extracted optical flow from the original SST image sequence. Figure 3 illustrates the extracted optical flow from SST images for which their contrast has been already enhanced.

4.3 Error Measurement

Combination of LSM parameters have been tested on both simulated and real motion images. The combination includes geometric transformation with 2, 4 and 6 parameters together with radiometric transformation with 0, 1 or 2 parameters (Table 1).

Table 1: Combination of geometric and radiometric parameters

	2 parameters	4 parameters	6 parameters
0	a_3, b_3	a_1, a_3, b_2, b_3	$a_1, a_2, a_3, b_1, b_2, b_3$
1	a_3, b_3, k_1	a_1, a_3, b_2, b_3, k_1	$a_1, a_2, a_3, b_1, b_2, b_3, k_1$
2	a_3, b_3, k_1, k_2	$a_1, a_3, b_2, b_3, k_1, k_2$	$a_1, a_2, a_3, b_1, b_2, b_3, k_1, k_2$

Velocity may be written as displacement per time unit as in $V = (u, v)$ pixels/frame, or as a space-time direction vector (u, v, 1) in units of (pixel, pixel, frame). Of course, velocity value in each direction is obtainable from the direction vector by dividing each element (*i.e.* u and v) to the third component (*i.e.* the number of intervals between the frames which is 1). When velocity is viewed (and measured) as orientation in space-time, it is natural to measure errors as angular deviations from the correct space-time orientation. Therefore, an angular measure of error has been used here. Let velocities $V = (u, v)^T$ be represented as 3D direction vectors.

$$\vec{V} \equiv \frac{1}{\sqrt{u^2 + v^2 + 1}}(u, v, 1)^T \quad (17)$$

The angular error between the correct velocity, $\vec{V}_c$, and an estimated one, $\vec{V}_e$, is

$$\psi_E = \arccos(\vec{V}_c . \vec{V}_e) \quad (18)$$

The error measure is contented because it handles large and very small speeds without the amplification inherent error in a relative measure of vector differences. It may also include some bias. For instance, directional errors at small speeds do not give as large angular error as similar directional errors at higher speeds. Table 2 shows result of average and standard deviation of angular error in the simulated motion analysis.

Table 2: Result of optical flow in simulated motion images

Transformed image			
Transformation		Average	Standard
Geometric	Radiometric	Error	Deviation
2	0	2.85°	2.29°
4	0	3.09°	2.53°
6	0	3.09°	2.56°
2	1	2.76°	2.27°
4	1	3.03°	2.44°
6	1	3.13°	2.58°
2	2	2.99°	2.49°
4	2	3.06°	2.53°
6	2	2.76°	1.97°

The optical flow extracted from contrast enhanced SST images generates smaller variation of mean error than optical flow extracted from the original SST images. This is because the enhanced SST images have wider range of gray values and therefore the least squares matching algorithm produces smoother vectors. This also helps in better interpretation of the water currents within the enhanced SST images.

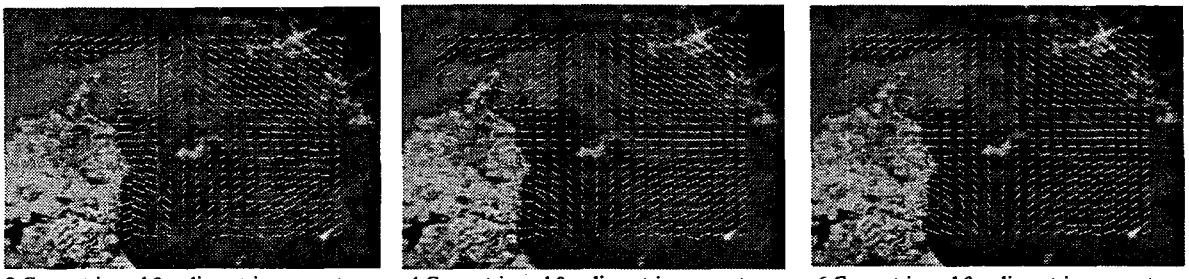
2 Geometric and 0 radiometric parameters 4 Geometric and 0 radiometric parameters 6 Geometric and 0 radiometric parameters

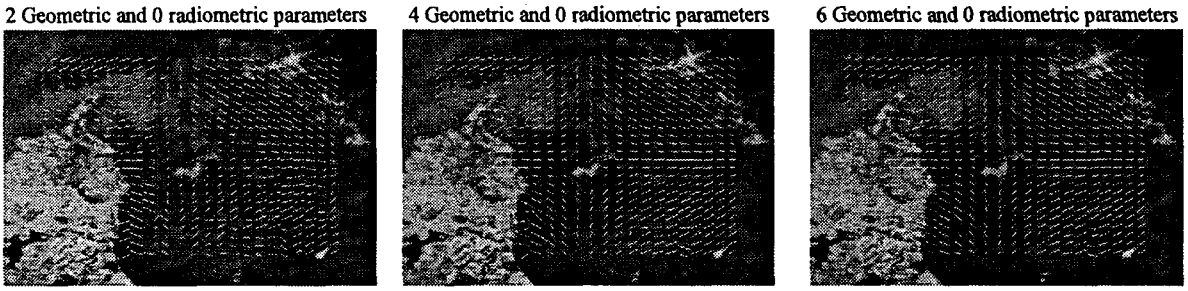
2 Geometric and 1 radiometric parameters 4 Geometric and 1 radiometric parameters 6 Geometric and 1 radiometric parameters

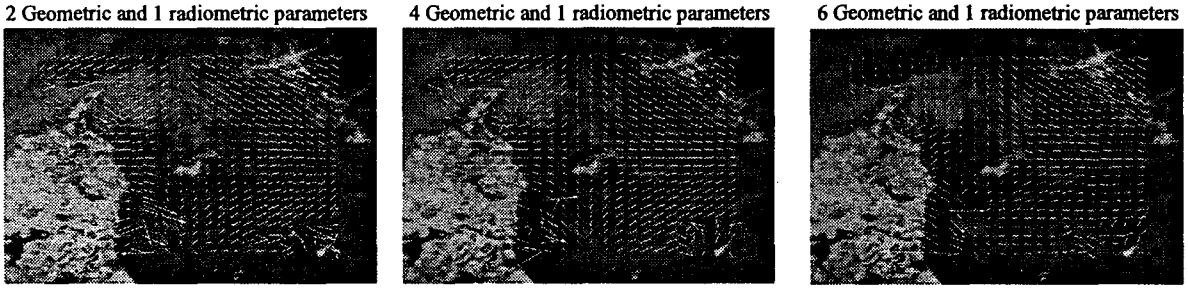
2 Geometric and 2 radiometric parameters 4 Geometric and 2 radiometric parameters 6 Geometric and 2 radiometric parameters

Figure 1: Optical flow from simulated motion image.

5. CONCLUSIONS

The least squares correlation has been utilized in an image matching process and optical flow extraction using MODIS data. As shown in this study, using daily SST images and exploiting temperature patterns as tracer of water bodies in Caspian Sea, the optical flow of the currents and motions has been generated by LSM. The reliability of LSM has been investigated by a combination of geometric and radiometric parameters. Also, the extraction of optical flow using contrast enhanced SST images has produced better result when compared to original SST sequences. The technique may be applied to similar data sets to analyze cloud motion and water vapor displacement.

Point tracing with grey level matching, has increased the precision and reliability of the matching procedure. Therefore, the technique offers a number of influence features, such as 1) high matching accuracy (*i.e.* sub-pixel accuracy), 2) monitoring of quality for which precision and reliability measures are easily available, 3) simultaneous geometrical image shaping and radiometric adjustment availability, and 4) its usability in a hierarchical mode (coarse-to-fine). Another advantage of the procedure is that the blunders have been controlled properly because of the existence of the criteria for checking iteration of least squares matching. In similar studies, a variety of geometrical constraints such as projective and DLT may be incorporated to support the grey level matching.

6. REFERENCES

Gruen, A.W, 1985, Adaptive least squares correlation: a powerful image matching technique, Journal of Photogrammetry, Remote Sensing and Cartography, 14 (3), pp.175-187.

Ackermann, F., 1988, Digital Image Correlation: Performance and Potential Application in Photogrammetry, presented at Thompson Symposium, Birmingham.

Bethel, J, 1997, Least squares image matching for CE604, Purdue University

Ackermann, F., 1983, High Precision Digital Image Correlation, Proceedings 39th Photogrammetric Week, Institute fur Photogrammetry, University at Stuttgart, Stuttgart,GER, Heft 9.

2 Geometric and 0 radiometric parameters | 4 Geometric and 0 Radiometric parameters | 6 Geometric and 0 Radiometric parameters

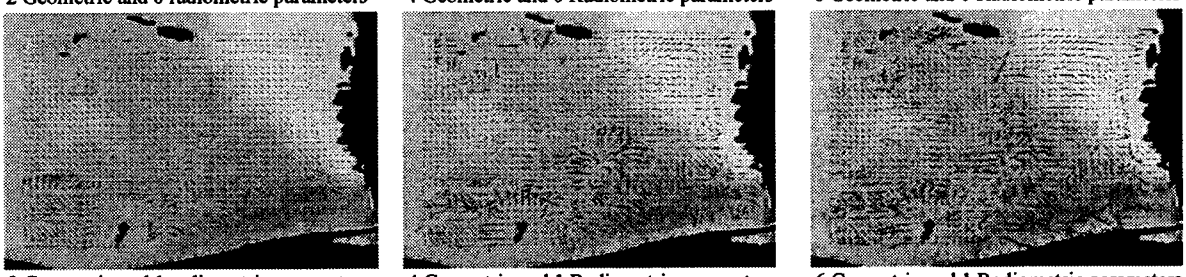

2 Geometric and 1 radiometric parameters | 4 Geometric and 1 Radiometric parameters | 6 Geometric and 1 Radiometric parameters

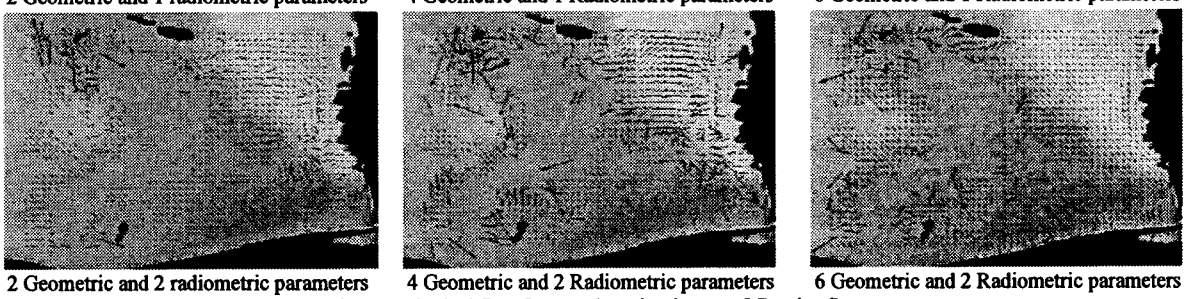

2 Geometric and 2 radiometric parameters | 4 Geometric and 2 Radiometric parameters | 6 Geometric and 2 Radiometric parameters

Figure 2: Optical flow from real motion image of Caspian Sea.

2 Geometric and 0 radiometric parameters | 4 Geometric and 0 radiometric parameters | 6 Geometric and 0 radiometric parameters

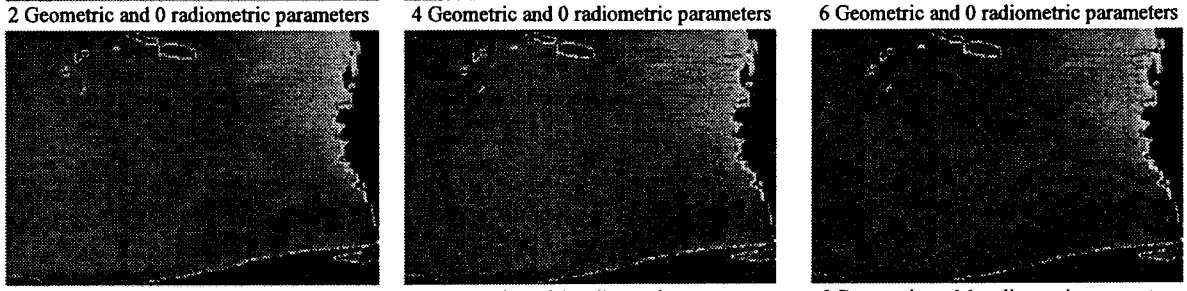

2 Geometric and 1 radiometric parameters | 4 Geometric and 1 radiometric parameters | 6 Geometric and 1 radiometric parameters

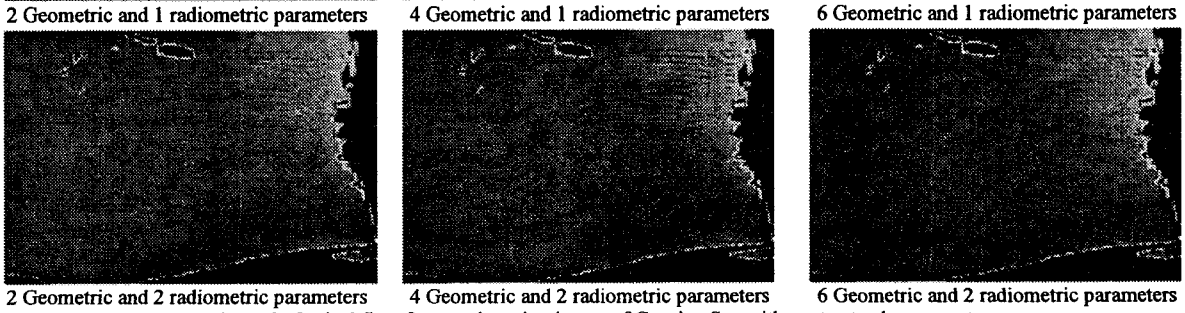

2 Geometric and 2 radiometric parameters | 4 Geometric and 2 radiometric parameters | 6 Geometric and 2 radiometric parameters

Figure 3: Optical flow from real motion image of Caspian Sea with contrast enhancement.